I&EC research
Industrial & Engineering Chemistry Research
pubs.acs.org/IECR
Article

Effect of Ligand Structure on the Kinetics of Heavy Oil Oxidation: Toward Biobased Oil-Soluble Catalytic Systems for Enhanced Oil Recovery

Abdolreza Farhadian, Mohammed A. Khelkhal,* Arash Tajik,* Semen E. Lapuk,* Morteza Rezaeisadat, Alexey A. Eskin, Nikolay O. Rodionov, and Alexey V. Vakhin*

Cite This: *Ind. Eng. Chem. Res.* 2021, 60, 14713−14727

Read Online

ACCESS | Metrics & More | Article Recommendations | Supporting Information

ABSTRACT: In recent years, protection of the environment from activities associated with enhanced oil recovery has been considered a crucial priority for decision-makers in the international community. The in situ combustion process as a promising thermal enhanced oil recovery method has been attracting considerable interest in terms of improving oil production and environmental protection. However, this technique is not yet well studied. This paper outlines a new approach to improve the process of heavy oil oxidation by designing new biobased oil-soluble catalysts that are able to maintain and stabilize the combustion flame front of the in situ combustion process. A comprehensive theoretical and experimental study including thermal analysis (thermogravimetry/differential scanning calorimetry, TG/DSC) and quantum calculations was used to shed light on the effect of the ligand structure in the oil-soluble catalytic system on the heavy oil oxidation process. The obtained accurate results proved that metal interaction with the designed ligands increased, which led to a decrease in the energy of activation and an increase in the heavy oil oxidation reaction rate. Besides, the obtained DSC curves showed one peak in the presence of Cu and biobased ligands, contrary to the curves obtained for heavy oil oxidation reported with other ligands and metals. In other words, the obtained catalysts merged low-temperature- and high-temperature oxidation regions into one region. These findings reveal that the structure of ligands can significantly affect their interaction with metals in oil-soluble catalysts, and therefore the efficiency of catalysts is dramatically improved. We believe that our work could be usefully employed for further studies to clarify the mechanism of the in situ combustion behavior of heavy oil for a better impact on the environment.

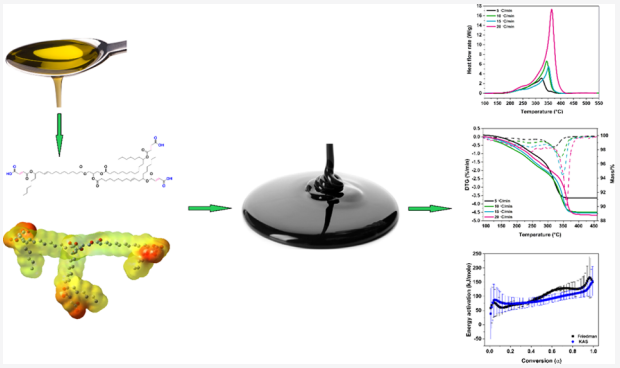

INTRODUCTION

Nowadays, increasing demand in the modern world for energy resources and the depletion of conventional oil reserves are widely seen to be the primary cause for moving toward finding new energy sources and developing new technologies for enhancing unconventional oil recovery.[1] It is common knowledge that a major part of the global oil reserves consists mainly of heavy oil and bitumen (60−70%), which, therefore, may meet the future needs of the world in terms of energy. However, the main limitation of this type of oils is their high viscosity and density, which challenge and complicate their exploitation and production.[2−4] Therefore, research on enhanced heavy oil recovery (EOR) methods is essential to increase the rate of heavy oil production on one hand and on the other hand to improve the quality of the obtained oil as well.[5] Until now, water injection, chemical injection, gas, and thermal injection have been considered the main proposed methods in the field of EOR.[6,7,16,8−15] However, thermal methods are widely believed to be the most important enhanced oil recovery methods in terms of the produced oil quality and economic aspects. According to the literature, in situ combustion (ISC) as a subset of the thermal injection method has been always considered as an effective and appropriate technology, especially when it comes to heavy oil reservoir exploitation.[17−23] Basically, this technology consists mainly of air injection into the reservoir under high pressure to provide the necessary conditions for initiating oxidation reactions and promoting a stable combustion flame front for a better oil recovery factor. Thus, it increases the reservoir pressure, reduces the viscosity of the crude oil, and decreases the possibility of the presence of sulfur and heavy metals, which leads to a significant improvement in oil mobility.[24] It is

Received: August 17, 2021
Revised: September 25, 2021
Accepted: September 28, 2021
Published: October 8, 2021

Downloaded via KAZAN FEDERAL UNIV on October 7, 2022 at 11:40:41 (UTC).
See https://pubs.acs.org/sharingguidelines for options on how to legitimately share published articles.

ACS Publications
© 2021 American Chemical Society

https://doi.org/10.1021/acs.iecr.1c03276
Ind. Eng. Chem. Res. 2021, 60, 14713−14727

Table 1. Physical Properties of Maiorovskoe Heavy Oil at 20 °C

		elemental content (%)					SARA analysis (%)			
viscosity (mPa s)	density (g cm^{-3})	C	H	N	S	O	saturated	aromatic	resins	asphaltenes
4600	0.95	83.7	10.2	0.4	3.8	1.9	25.7	39.0	23.9	11.4

worthy to note that the combustion flame front is widely seen as the main key for the successful application of any in situ combustion project. Moreover, many scientists have described heavy oil in situ combustion as a process that passes through three basic stages. In fact, it is initiated by a low-temperature oxidation (LTO) process during which oxygen combines with heavy oil content and results in oxygenated compounds such as alcohols, ketones, and aldehydes. Next, the obtained hydrocarbons at low-temperature oxidation condense and form what is known in the literature as fuel deposits (FDs). This stage is known as medium-temperature oxidation. Finally, the obtained fuel deposits (FDs) or in a large number of studies known as coke undergo oxidation at higher temperatures in the stage called the high-temperature oxidation (HTO) region.[13,18,25−27] One of the main issues as per our knowledge of in situ combustion is a lack of a clear explanation of the early breakthrough of the combustion flame front after a short time of initiating the combustion, which majorly leads to the failure of most in situ combustion projects. Some preliminary works were carried out several years ago to study the real causes of combustion flame front instability using various catalysts such as transition metal (TM)-based compounds, metal oxides, water-soluble metals, oil-soluble metals, and minerals such as clay.[28−33] It is worthwhile noting that TMs and their oxides have received much attention for thermal EOR due to their high capacity for adsorption and activation of oxygen,[29] as well as their contribution to the propagation steps to regenerate more free radicals during oxidation processes. In addition, their high heat transfer coefficient can increase the efficiency of thermal oil recovery processes.[34] Recent findings regarding metal nanoparticles have led to the discovery of their significant role in promoting the thermal recovery of heavy oil.[35,36] In their investigation of the impact of copper nanoparticles on the ISC process of heavy crude oil, Amanam et al. have shown that copper nanoparticles have a significant influence on the apparent activation energy of the HTO region and the fuel formation zone.[37] The first systematic studies on catalytic EOR methods have proposed to classify the adopted catalysts into water-soluble and oil-soluble catalysts. In fact, both types of catalysts usually contain metals such as Ni, Cu, Co, and Mo,[38] which bind as metal salts or chemically bind to organic ligands such as carboxylates, sulfonates, and ionic liquids. However, TM carboxylate with the general formula $(R\text{-}COO^{-})^{n}$ $(TM)^{n+}$ has been used as one of the first catalysts for heavy oil recovery due to its cost-effectiveness and ligand availability. Moreover, TM carboxylate can be synthesized by neutralizing carboxylic acids with metal hydroxides or ion exchange of sodium carboxylates with metal salts at low temperatures. Generally, TM carboxylates including alkyl carboxylates (or mixtures thereof), oleates, and naphthenates can serve as excellent catalysts compared to water-insoluble inorganic salts to reduce the viscosity of heavy oils.[39−43] Another reason for the efficiency of oil-soluble TM carboxylates is the proper dispersion in heavy oil, which prevents coke formation and allows for more efficient interaction with oil components.[44] The literature reveals that the use of oil-soluble organic ligands in ISC can increase the lipophilic nature of the catalysts (improve solubility in oil), bring TM to the surface, and even the internal phase of the heavy oil.[34] Khelkhal et al. showed an acceptable effect of copper-manganese tallates in stabilizing the combustion flame front during oxidation reactions at high temperatures by means of thermal analysis.[45] They also reported in other studies that both nickel and cobalt tallates significantly reduced the activation energy of the HTO region and increased the effective reaction rate constant.[31] Yuan et al. demonstrated that copper stearate shifted the low-temperature oxidation peak by around 50 °C at the onset and peak temperatures.[26] Although several oil-soluble catalysts have been widely investigated for heavy oil recovery, research unfortunately has tended to focus on their effect on the recovery factor and in some cases on the nature of the metal used. An additional drawback is that most of the previous studies have used a simple ligand that consisted only of a long alkyl chain and a carboxylate ion. In other words, the effect of the ligand structure on the kinetics of heavy oil oxidation in the presence of oil-soluble catalysts has not been studied so far. Moreover, there is still considerable neglect, unfortunately, from the research community in designing green and environment-friendly catalysts to enhance heavy oil recovery on one hand and on the other hand to protect the environment and the planet. The aim of the present work is to cover this gap by designing two new environment-friendly, biodegradable ligands based on vegetable oil to provide new insight into interactions between ligand and metal in oil-soluble catalysts and their effect on the oxidation of heavy oil for the first time. The performance of these oil-soluble catalysts based on novel green ligands and their effect on the kinetics of the heavy oil oxidation process were evaluated using differential scanning calorimetric (DSC) and thermogravimetric (TGA) analyses. Moreover, a theoretical study based on quantum calculation was carried out to support experimental results and investigate the ligand−metal interactions with different metals.

EXPERIMENTAL SECTION

Materials. The studied heavy oil was kindly provided by RITEK (R&D test site for Lukoil company) from the Maiorovskoe oilfield (Volga Federal District, Samara region, Russia) and is described in Table 1. Castor oil (CO), succinic anhydride (SA), maleic anhydride (MA), ethanol, $CuSO_4 \cdot 5H_2O$, and $Ni(NO_3)_2 \cdot 6H_2O$ were purchased from Sigma Co.

Preparation of Castor Oil-Based Ligands (COLs). Two COLs were synthesized by reaction of castor oil with different anhydride compounds. Maleic anhydride and succinic anhydride were used for synthesizing COL1 and COL2, respectively. Literally, the preparation method of both ligands basically consists of an esterification reaction as described in the literature.[46,47] COL2 was synthesized as follows. Briefly, 50 g (0.51 mol) of MA and 158 g (0.17 mol) of CO were added to a 500 mL single-neck round-bottom flask fitted with a condenser. The reaction was carried out at 110 °C for 12 h. Finally, the reaction mixture was washed with deionized water three times to eliminate the unreacted MA. The chemical structures of COL1 and COL2 are depicted in Figure 1. The

https://doi.org/10.1021/acs.iecr.1c03276
Ind. Eng. Chem. Res. 2021, 60, 14713−14727

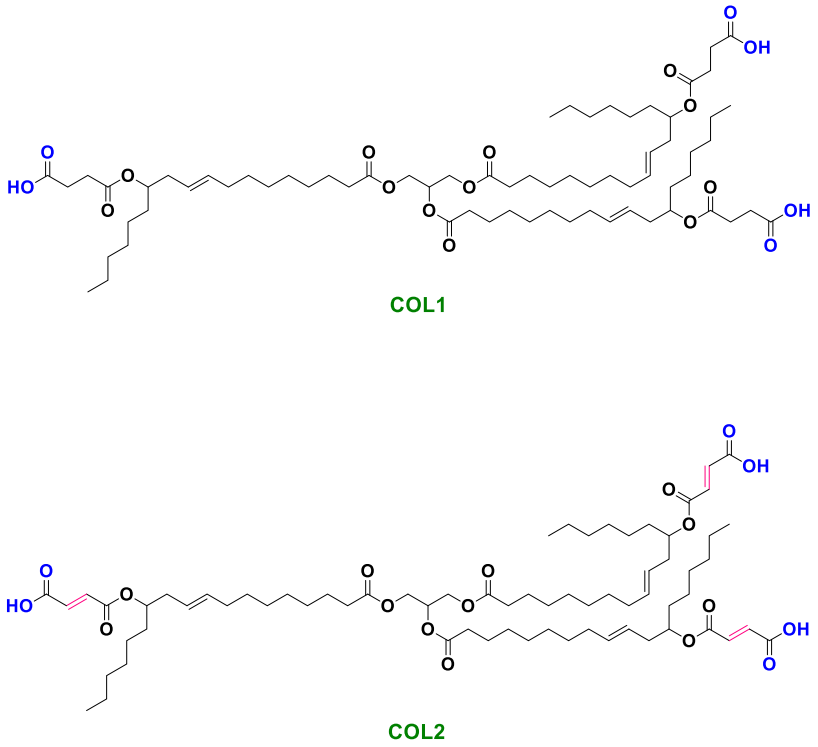

Figure 1. Chemical structure of castor oil-based ligands (COLs).

chemical structure of synthesized ligands was characterized using a Bruker Avance 400 MHz. ^{1}H NMR (400 MHz, DMSO-d_6) spectrum of COL1: δ 6.39−6.23 (m, 3H), 5.51−5.23 (m, 3H), 5.19 (dq, J = 6.8, 3.3 Hz, 1H), 4.84 (t, J = 6.1 Hz, 1H), 4.26 (dd, J = 12.0, 3.7 Hz, 1H), 4.12 (dd, J = 12.0, 6.5 Hz, 1H), 2.90 (s, 6H), 2.74 (s, 4H), 2.51 (t, J = 2.0 Hz, 1H), 2.27 (t, J = 7.3 Hz, 6H), 2.07 (q, J = 6.1 Hz, 0H), 1.98 (p, J = 6.8 Hz, 4H), 1.51 (q, J = 6.8 Hz, 6H), 1.24 (d, J = 7.9 Hz, 31H), 0.84 (t, J = 6.5 Hz, 5H).

^{1}H NMR (400 MHz, DMSO-d_6) spectrum of COL2: δ 5.42 (q, J = 7.8 Hz, 2H), 5.36−5.24 (m, 3H), 5.19 (t, J = 5.1 Hz, 1H), 4.76 (q, J = 6.1 Hz, 2H), 4.26 (dd, J = 12.2, 3.6 Hz, 2H), 4.11 (dd, J = 11.9, 6.4 Hz, 2H), 4.03 (d, J = 7.1 Hz, 0H), 2.95 (s, 0H), 2.80 (s, 0H), 2.45 (s, 11H), 2.25 (dt, J = 14.1, 7.1 Hz, 12H), 1.98 (q, J = 6.3, 5.4 Hz, 7H), 1.49 (dt, J = 13.0, 6.7 Hz, 13H), 1.34−0.89 (m, 78H), 0.83 (d, J = 7.0 Hz, 24H).

Preparation of Oil-Soluble Catalysts. Metal salts ($CuSo_4{\cdot}5H_2O$ and $Ni(NO_3)_2{\cdot}6H_2O$) and the desired ligands were used in a molar ratio of 1:3 for the preparation of all oil-soluble catalysts. Ligand 1 or 2 was dissolved in ethanol and mixed with a mechanical stirrer for 20 min at room temperature. After a while, the pH of the ligand solution was adjusted to 10 using NaOH solution, and the solution became cloudy. Then, the metal salt−ethanol solution was added dropwise to the ligand solution. Finally, the mixture was stirred for 30 min, filtered, and washed three times with ethanol. The resulting precipitate was dried at ambient temperature for 18 h. In the end, four oil-soluble catalysts (OSCs) were obtained, namely, Cu+COL1 (OSC1), Ni+COL1 (OSC2), Cu+COL2 (OSC3), and Ni+COL2 (OSC4).

Sample Preparation for Thermal Analysis. To study the noncatalytic oxidation, heavy oil (10.0 wt %) was mixed with a pure quartz sand fraction of 43−64 μm (90.0 wt %). However, for studying the catalytic oxidation process, heavy oil with catalyst (10.0 wt %) was mixed with the pure quartz sand fraction of 43−64 μm. The content of the catalyst was 2 wt % in the initial oil. The shape and particle size of nanoparticles before oxidation were also investigated using a Tescan Mira3 (Brno, Czech Republic) at an accelerating voltage of 30 kV without gold coating.

Thermal Analysis. An STA 449 F1 Jupiter (Netzsch) thermoanalyzer at a temperature range of 30−600 °C with heating rates of 5, 10, 15, and 20 °C/min and a 50 mL/min air flow was used to estimate the kinetic parameters of the heavy oil oxidation process by means of simultaneous differential scanning calorimetry (DSC) and thermogravimetric analysis (TGA). The Proteus Analysis v5.2.1 and NETZSCH Kinetics Neo 2.1.2.2 program package were used to treat and interpret the obtained data. Many experts in the field of heavy oil oxidation consider using nonisothermal kinetic methods rather than using isothermal kinetic analysis due to the exothermic nature of the process and the heterogeneous aspect of the heavy oil combustion process. In other words, the medium in which the process occurs includes three phases: gas, liquid, and solid components. As a consequence, heavy oil has acquired a complex aspect in terms of understanding the mechanisms involved during its combustion, especially in situ and in the presence of other species. Besides, this process not only requires the study of the kinetic aspects but also calls out to interdisciplinary studies such as understanding thermodynamics and diffusion processes accompanying it.

Kinetic Analysis. During this work, we studied the process of heavy oil oxidation and the relation between the nature of the transition metal and the ligands in the catalyst system in addition to their effect on the kinetic parameters of the process of oil oxidation based on the recommendations of ICTAC. To determine the kinetic parameters, the isoconversional and model approaches of nonisothermal kinetics were used.[48,49] All isoconversional methods originate from the isoconversional principle, which states that the reaction rate at a constant

https://doi.org/10.1021/acs.iecr.1c03276
Ind. Eng. Chem. Res. 2021, 60, 14713−14727

conversion is only a function of temperature. The following isoconversional approaches were used in the present work: Kissinger's method (ASTM E2890),[50] Friedman's analysis,[51] and the Kissinger–Akahira–Sunose method. Selection of the model was carried out by minimizing the effect of the difference between the experimentally measured and the calculated data on the reaction rate.[48] In fact, the models used in the model approach are presented in Table 2. Evaluation of the catalyst efficiency was based on the predicted conversion times at different degrees of conversion.[52,53]

Table 2. Models' Methods for Calculating Kinetic Parameters

model	equation
reaction of nth order (Fn)	$f = (1 - \alpha)^n$ (1)
N-dimensional nucleation according to Avrami–Erofeev (An)	$f = n\cdot(1 - \alpha)\cdot[-\ln(1 - \alpha)]^{(n-1)/n}$ (2)
expanded Prout–Tompkins equation (Bna)	$f = (1 - \alpha)^n\cdot\alpha^{\text{AutocatOrder}}$ (3)
reaction of nth order with m-power autocatalysis by product (Cnm)	$f = (1 - \alpha)^n\cdot(1 + \text{AutocatOrder}\cdot\alpha^m)$ (4)

Computational Method. The initial structures of COL2, oleic acid (as a common ligand structure for previous studies of oil-soluble catalysts), Cu, and Ni clusters were drawn using the Gaussview06 program and fully optimized using Gaussian09[54] software and density functional theory[55] with hybrid exchange–correlation B3LYP functional.[56] The Dunning[57] double-zeta correlation-consistent basis sets plus diffusion functions (aug-cc-pvdz) for all structures were applied. Calculations were performed in the water medium, and for this purpose, the PCM (polarizable continuum model) water model was used.[58] Some useful properties and energies related to each of the optimized structures were obtained. The binding energy (E_b) of the Cu–ligand complex is defined as follows[59]

$$E_b = E_{\text{Cu-ligand}} - (E_{\text{Cu-cluster}} - E_{\text{ligand}}) \quad (5)$$

where $E_{\text{Cu-ligand}}$, $E_{\text{Cu-cluster}}$, and E_{ligand} are related to the energy of the Cu cluster and the ligand complex, the energy of the triple Cu cluster, and the ligand energy, respectively. These calculations were also used for Ni to evaluate and compare the binding energies between nickel and copper metal clusters with COL2. Another property that was considered in this study was related to the energy gap, which is the difference between the highest occupied molecular orbital (HOMO) and the lowest unoccupied molecular orbital (LUMO) as follows

$$E_{\text{gap}} = E_{\text{LUMO}} - E_{\text{HOMO}} \quad (6)$$

The effect related to the correction of the base set superposition error (BSSE)[60] in the formation of the complex of Cu cluster with the ligand was reduced to ~0.007 H. Natural bond orbital (NBO) and quantum theory of atoms in molecules (QTAIM) analysis were utilized to investigate the nature of the interaction of the Cu cluster with the ligand. The NBO analysis was used to obtain natural partial charge changes and charge transfers associated with the complexes.[61,62] The QTAIM analysis was carried out using the AIM2000 software package.[63,64] These calculations are carried out to obtain the properties of bond critical points (BCPs).

RESULTS AND DISCUSSION

Many experts now argue that it might be more useful to initiate heavy oil oxidation studies at small scales using differential scanning calorimetric analysis combined with thermogravimetric analysis, which provides accurate data about the effect of different substances on the processes of thermal degradation such as the heavy oil oxidation process, rather than applying newly synthesized catalysts in the field at larger scales. Besides, the thermal analysis presents a particular interest in terms of time consumption, cost, and design. Hence, we are able to investigate the process of heavy oil oxidation in the absence and presence of the obtained biobased catalysts. Figures 2–4 demonstrate the obtained DSC curves for oxidation of the heavy oil, OSC1–OSC2, and OSC3–OSC4 systems.

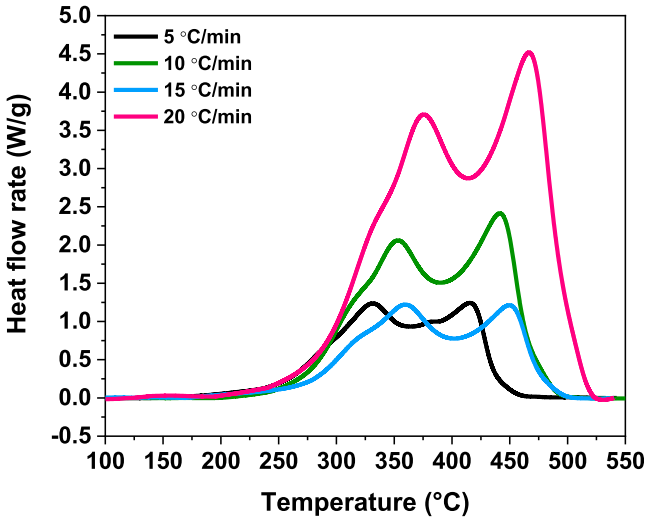

Figure 2. DSC curves for heavy oil noncatalytic oxidation at different heating rates.

The DSC analysis highlighted the impact of adding different catalysts with different compositions on the process of heavy oil oxidation. In fact, the nature of the ligand played a crucial role in changing the behavior of the process of oil oxidation. It is common knowledge that the process of oil oxidation includes two different zones, mainly low-temperature oxidation (LTO) and high-temperature oxidation zones, as presented by the two peaks in the DSC peaks at different heating rates (Figure 2). During low-temperature oxidation, the injected oxygen reacts with oil components and forms oxygenated compounds such as ketones, aldehydes, and alcohols,[65] while the high-temperature oxidation zone includes the process of coke combustion.[65] Interestingly, the behavior of the oil oxidation process in some cases was changed and displayed almost one main peak (Figure 3a) and absolutely one peak (Figure 4a) in the presence of OSC1 and OSC3, respectively. The current study does not support previous research in this area. In fact, unlike what was previously thought, we found that the nature and the structure of the ligand in addition to the nature of the associated metal may change the whole mechanism of heavy oil oxidation, and this is shown in Figures 3a and 4a. Moreover, a considerable peak-temperature displacement effectively took place in the presence of all added catalysts during high-temperature oxidation regardless of the nature of ligands or metals at different heating rates. It is worthy to note that the high-temperature oxidation zone is

https://doi.org/10.1021/acs.iecr.1c03276
Ind. Eng. Chem. Res. 2021, 60, 14713–14727

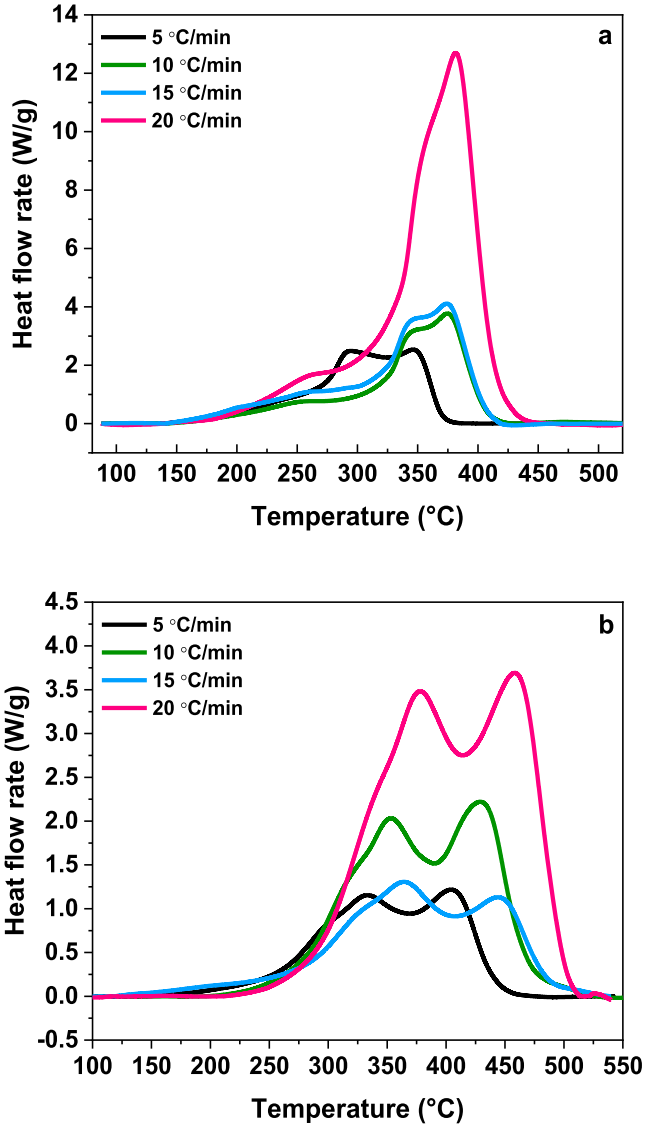

Figure 3. DSC curves for heavy oil catalytic oxidation in the presence of OSC1 (a) and OSC2 (b) based on COL1 at different heating rates.

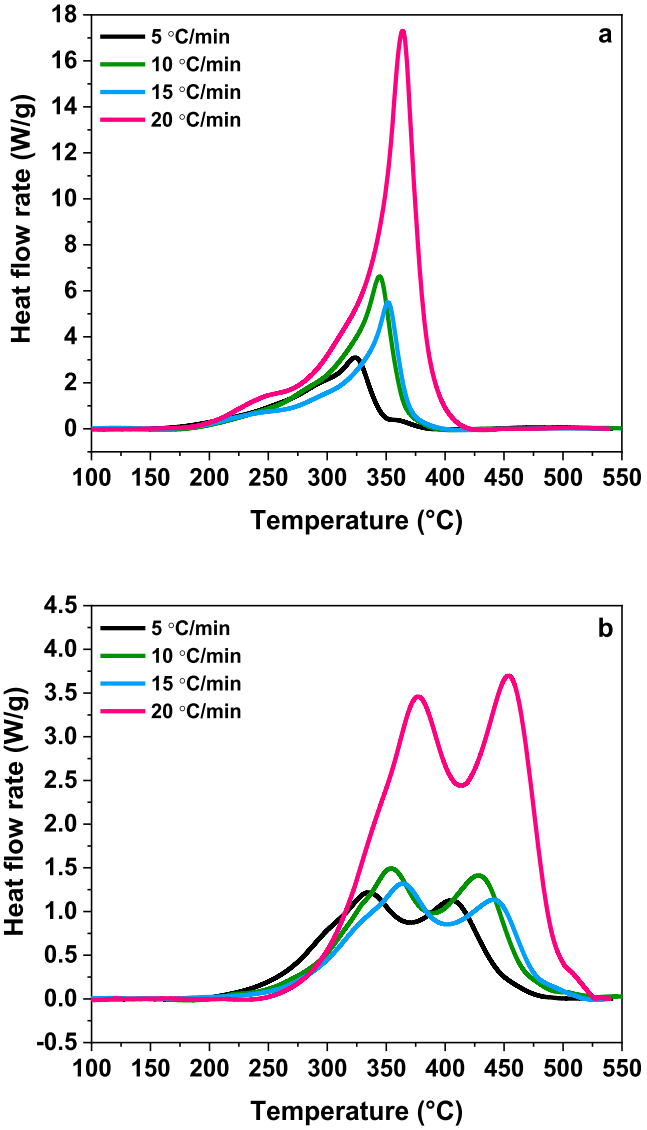

Figure 4. DSC curves for heavy oil catalytic oxidation in the presence of OSC3 (a) and OSC4 (b) based on COL2 at different heating rates.

widely believed to be key in the successful application of the in situ combustion process since it is the region in which the combustion flame front stabilizes and generates more heat and thermal energy to the rest of the reservoir.[13,19,32] Thereby, we focused mainly, during our investigation, on the impact generated by the synthesized catalysts on this region. To confirm our hypothesis, we implemented thermogravimetric analyses and treated the obtained data carefully to construct differential thermal gravimetric curves as displayed in Figures 5−7.

At a glance, it seems that the influence of OSC1 and OSC3 on the oxidation behavior of heavy oil oxidation is insignificant. However, a closer inspection of thermal gravimetric curves and their associated differential thermal gravimetric analysis has confirmed our hypothesis of the role of OSC1 and OSC3 in changing the dynamics of the heavy oil oxidation process curves by eliminating both LTO and HTO and merging them in one process, which presents only by one peak on both DSC and TG/DTG curves. Another interesting fact that emerged from the obtained TG/DTG curves is the appearance of a third peak in the presence of OSC2 and OSC4 in a more

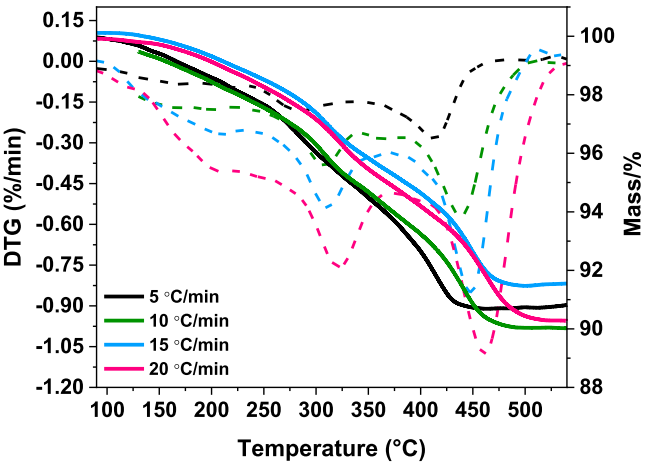

Figure 5. Thermogravimetric (TG) and differential thermogravimetric (DTG) curves for heavy oil noncatalytic oxidation at different heating rates.

https://doi.org/10.1021/acs.iecr.1c03276
Ind. Eng. Chem. Res. 2021, 60, 14713−14727

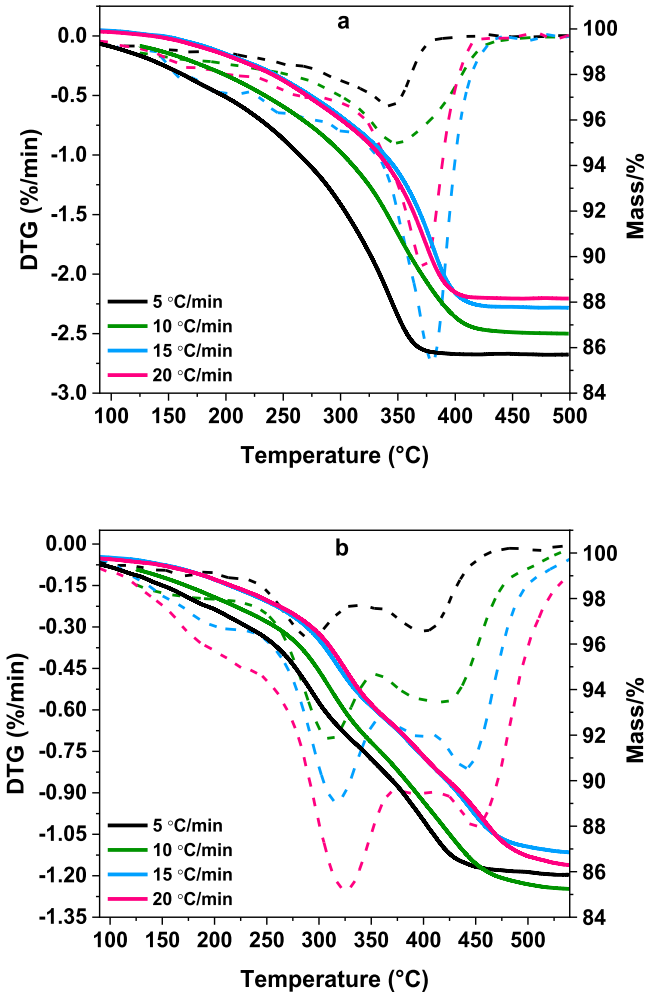

Figure 6. Thermogravimetric (TG) and differential thermogravimetric (DTG) curves for heavy oil catalytic oxidation in the presence of OSC1 (a) and OSC2 (b) based on COL1 at different heating rates.

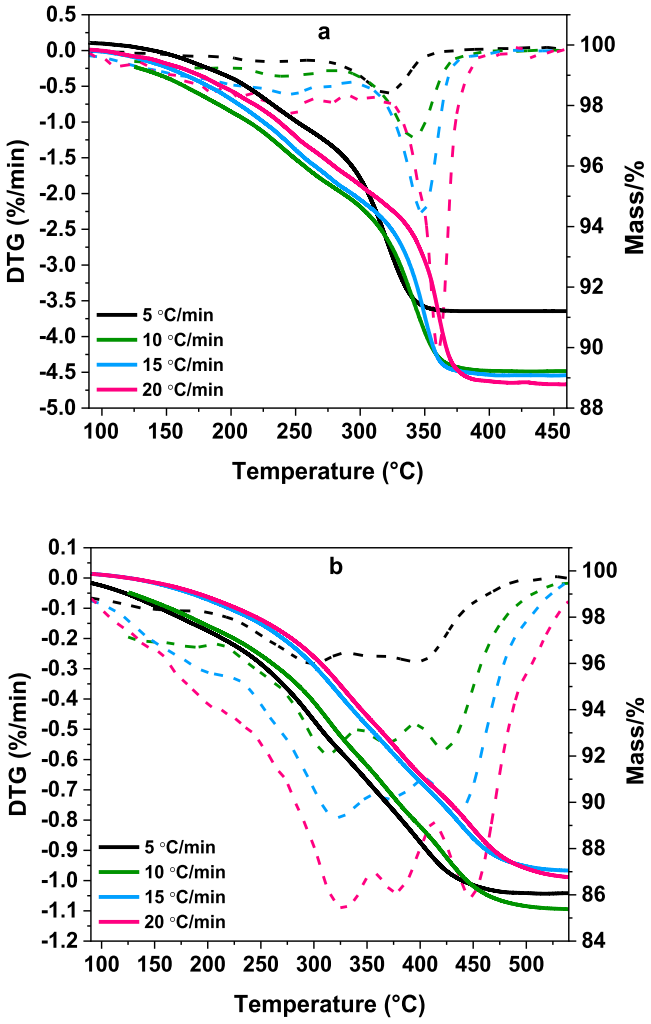

Figure 7. Thermogravimetric (TG) and differential thermogravimetric (DTG) curves for heavy oil catalytic oxidation in the presence of OSC3 (a) and OSC4 (b) based on COL2 at different heating rates.

intense manner. Moreover, the obtained TG/DTG curves are in good agreement with the DSC curves. Given that our findings are based on a limited number of observations provided by DSC/TG analysis, the results from such analysis should thus be treated with considerable caution. These findings were further strengthened by calculating the kinetic parameters of the process of heavy oil oxidation in the presence and the absence of the synthesized catalysts.

Kinetic Study. To understand the effect of the new catalysts on the heavy oil oxidation process, the dependencies of the activation energy and the pre-exponential factor on the degree of conversion were studied by the Kissinger methods (ASTM E2890), Friedman analysis, and the Kissinger–Akahira–Sunose method. The Kissinger method (ASTM E2890) was applied to eliminate the reaction model from the kinetic equation. The values of energy of activation and the pre-exponential factor in different oil oxidation regions can be determined by means of Kissinger curves (Figure 8) in the presence and the absence of the synthesized catalysts. The calculated kinetic parameters are presented in Table 3.

The most striking results to emerge from Table 3 are the significant effect of almost all of the added catalysts on decreasing the energies of activation of both regions (LTO and HTO), except when catalyst OSC1 was added to the sample of oil where, unlike other catalysts, it increased the value of the HTO-region activation energy. Even though the catalysts decreased the activation energies for the heavy oil oxidation process, which is considered a significant index for their efficiency, their effect, however, on the pre-exponential factor was in contradiction to that on the values of activation energies. In other words, the obtained values of pre-exponential factors decreased in the presence of OSC2 and OSC4, which might decrease the reaction rate constant. However, OSC1 and OSC3 showed higher values of pre-exponential factors, which leads to an increase in the reaction rate constants, especially for sample OSC3, which in addition to this effect decreased the value of the energy of activation. A low activation energy value and a high pre-exponential factor in the presence of OSC3 imply its higher oxidation rate constant. It is well known that the activation energy and the pre-exponential factors are inversely proportional to the reaction rate values.[31−33] Activation energy dependency on conversion degree obtained by Friedman analysis and the KAS method is shown in Figure 9.

As seen from Figure 9, a significant variation in the values of activation energy with increasing conversion degree is present in the graphs of Friedman and KAS analyses. In fact, the so-called "shoulders" present in the obtained graphs exhibit a multistep process of heavy oil oxidation, both in pure form and

https://doi.org/10.1021/acs.iecr.1c03276
Ind. Eng. Chem. Res. 2021, 60, 14713−14727

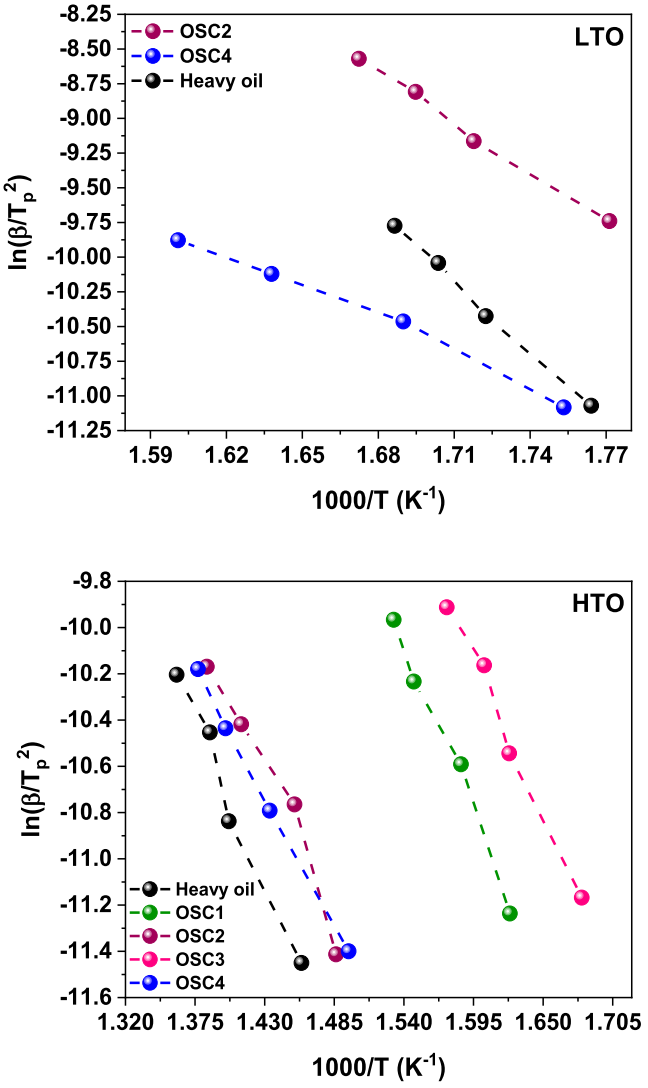

Figure 8. Kissinger plots for catalytic and noncatalytic heavy oil oxidation in low- and high-temperature oxidation regions.

Table 3. Kinetic Parameters of the Oil Oxidation Process in the Presence and the Absence of Catalysts

	E_a (kJ/mol)		ln(A) (A, min^{-1})	
sample	LTO	HTO	LTO	HTO
heavy oil	154.7 ± 8.8	106.9 ± 11.1	18.6	7.2
OSC1		110.5 ± 9.0		10.4
OSC2	99.3 ± 4.7	97.1 ± 14.9	11.4	6
OSC3		100.3 ± 7.9		9.1
OSC4	65.2 ± 4.9	84.4 ± 1.9	2.7	3.8

in the presence of a catalyst. This fact is also confirmed by DSC data, which show two peaks of oxidation: LTO and HTO. Moreover, the use of the isoconversional approach for multistep reactions does not always accurately reflect the effective reaction rate for each of the processes, as a consequence of which it is difficult to assess the effect of the catalyst on the LTO and HTO processes. Therefore, a model approach was used for the two-stage oxidation of heavy oil in the presence and absence of the catalyst to evaluate the effect of the catalyst on different oxidation regions. For each experiment on the oxidation of heavy oil, a selection of 16 two-step models was used. In fact, for each reaction step, we selected the corresponding model from Table 2. In addition, the selection of an optimal model that describes two-step reactions was performed using an F-test.[66] Table 4 shows the models providing the F-test value of 1.000. Detailed consideration of each of the calculated models is presented in Supporting Information S1.

The obtained model approach data associate the oxidation process with the autocatalytic models of Bna and Cnm. It has been shown that the activation energy of LTO decreases in the presence of catalysts OSC1, OSC2, and OSC3. However, there is a decrease in the pre-exponential factor for these catalysts as well compared to the noncatalytic process. Also, a decrease in activation energy for HTO has been observed only in the presence of OSC2. Therefore, to determine the effect of the catalysts on both LTO and HTO regions, we calculated the oil conversion time versus temperature for different degrees of conversion using the models obtained from Table 4.

Kinetic Predictions. The effect of catalyst on the heavy oil oxidation rate was determined from the predicted conversion times calculated using a model approach. For this, we calculated the associated times for 10, 50, and 90% of heavy oil oxidation. It was found that 10% corresponds to the beginning of the LTO process, 50% corresponds to the beginning of the HTO and the end of LTO, and 90% corresponds to the end of the HTO process as illustrated by Figure 10. It is assumed that short half-lives correspond to a high rate of the oxidation process, which in turn stabilizes the combustion flame front in the oil reservoir.

Interestingly, Figure 10 obviously highlights the effect of different catalysts with different compositions on the process of heavy oil oxidation. The most remarkable result from the obtained values for oxidation effective constant rates is the dramatic effect generated by OSC1 and OSC3, which share common characteristics in terms of containing the same metal (Cu) and different ligands and which increases the oxidation rate. In fact, higher values of the reaction rate were achieved by the addition of the synthesized OSC1 and OSC3 compared to those reported by several studies on the heavy oil oxidation process. In addition, the important role played by OSC1 and OSC3 can be seen from Figure 10, which indicates that the values of the reaction rate in the presence of OSC2 and OSC4 did not have a significant impact on the process of heavy oil oxidation rate constants in both LTO and HTO regions. To the best of our knowledge, this is the first time where the heavy oil oxidation process changes its common behavior known in the literature by merging two main regions (LTO and HTO) into a unique region (as presented by one peak in TG/DSC curves) in the presence of special ligands present in OSC1 and OSC3. These results strengthened our convenience in developing new ligands for preparation of biocatalysts to achieve better results in biobased enhanced oil recovery.

FESEM Study. Since the results of TGA and DSC experiments clearly confirmed that the kinetics of heavy oil oxidation can be strongly affected by the structure of ligands, a FESEM study was carried out to investigate the morphology and the size of metals in the oil-soluble catalyst before oxidation. OSC3 and OSC4 were selected for the FESEM analysis because these catalysts based on COL2 showed the best performance in the oxidation process. The morphology and the frequency of the particle size of Cu and Ni nanoparticles in OSC3 and OSC4 are depicted in Figures 11 and12, respectively. As seen in Figure 11, Cu nanoparticles are

https://doi.org/10.1021/acs.iecr.1c03276
Ind. Eng. Chem. Res. 2021, 60, 14713−14727

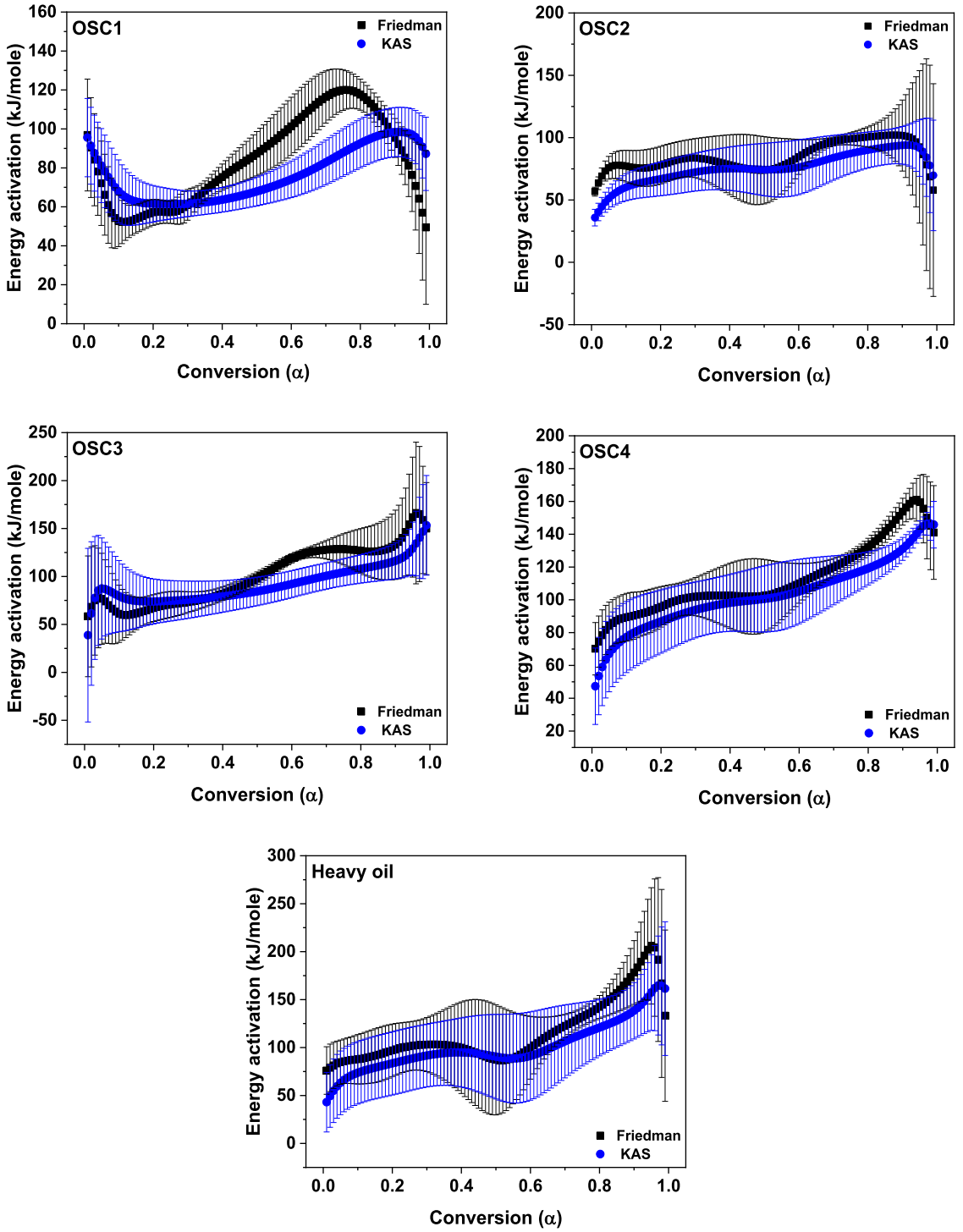

Figure 9. Graphs of activation energy dependency on conversion degree obtained by Friedman and the KAS method for (a) OSC1, (b) OSC2, (c) OSC3, (d) OSC4, and (f) heavy oil.

more spherical than Ni, which can provide a better contact surface with oil and increase the oxidation efficiency. Moreover, the percentage of the particle size frequency in Figure 12 shows that the size of most copper nanoparticles in OSC3 is less than 40 nm, while most nickel nanoparticles are in the range of 92−162 nm. It has been reported that[67,68] the size of nanoparticles has a significant effect on the heat transfer coefficient so that the smaller nanoparticles remarkably increase heat transfer. This can be caused by an increase in the surface area of the nanoparticles, which intensifies the random motion and collision between the nanoparticles and the fluid molecules. From these statistical data, it can be concluded that the nanoparticles of Cu have the ability to increase the oxidation efficiency of oil due to their smaller particle size compared to nanoparticles of Ni.

Theoretical Study. Since OSC3 among the four oil-soluble catalysts studied showed the best performance in heavy oil oxidation, COL2 was selected to investigate its interaction with Cu and Ni clusters. The physical and chemical properties of metal clusters strongly depend on their size; therefore, the

https://doi.org/10.1021/acs.iecr.1c03276
Ind. Eng. Chem. Res. 2021, 60, 14713−14727

Table 4. Kinetic Parameters of the Heavy Oil Oxidation Process in the Presence and Absence of Catalysts Obtained by the Model Approach of Nonisothermal Kinetics

	OSC1	OSC2	OSC3	OSC4	Heavy oil
	Cnm: E = 64.3 kJ/mol, lg A = 3.2 s^{-1}, ReactOrder n = 1.03, AutocatOrder 0.873, AutocatPower m = 3.828	Bna: E = 76.4 kJ/mol, lg A = 4.2 s^{-1}, ReactOrder n = 1.40, AutocatOrder 0.281	Cnm: E = 58.5 kJ/mol, lg A = 2.5 s^{-1}, ReactOrder n = 0.47, AutocatOrder 0.11, AutocatPower m = 0.01	Cnm: E = 101.3 kJ/mol, lg A = 6.2 s^{-1}, ReactOrder n = 1.47, AutocatOrder 0.23, AutocatPower m = 2.577	Cnm: E = 99.3 kJ/mol, lg A = 5.7 s^{-1}, ReactOrder n = 1.2, AutocatOrder 0.33, AutocatPower m = 0.395
	Bna: E = 125.8 kJ/mol, lg A = 8.4 s^{-1}, ReactOrder n = 1.05, AutocatOrder 0.313	Cnm: E = 93.9 kJ/mol, lg A = 4.2 s^{-1}, ReactOrder n = 1.0, AutocatOrder 0.68, AutocatPower m = 0.822	Cnm: E = 111.6 kJ/mol, lg A = 6.8 s^{-1}, ReactOrder n = 1.56, AutocatOrder 1.05, AutocatPower m = 1.049	Cnm: E = 112.9 kJ/mol, lg A = 6.1 s^{-1}, ReactOrder n = 1.53, AutocatOrder 0.505, AutocatPower m = 2.19	Cnm: E = 113.7 kJ/mol, lg A = 6.0 s^{-1}, ReactOrder n = 1.37, AutocatOrder 0.5, AutocatPower m = 1.763
R^2	0.99474	0.99646	0.99676	0.99764	0.9935
F-test	1.000	1.000	1.000	1.000	1.000

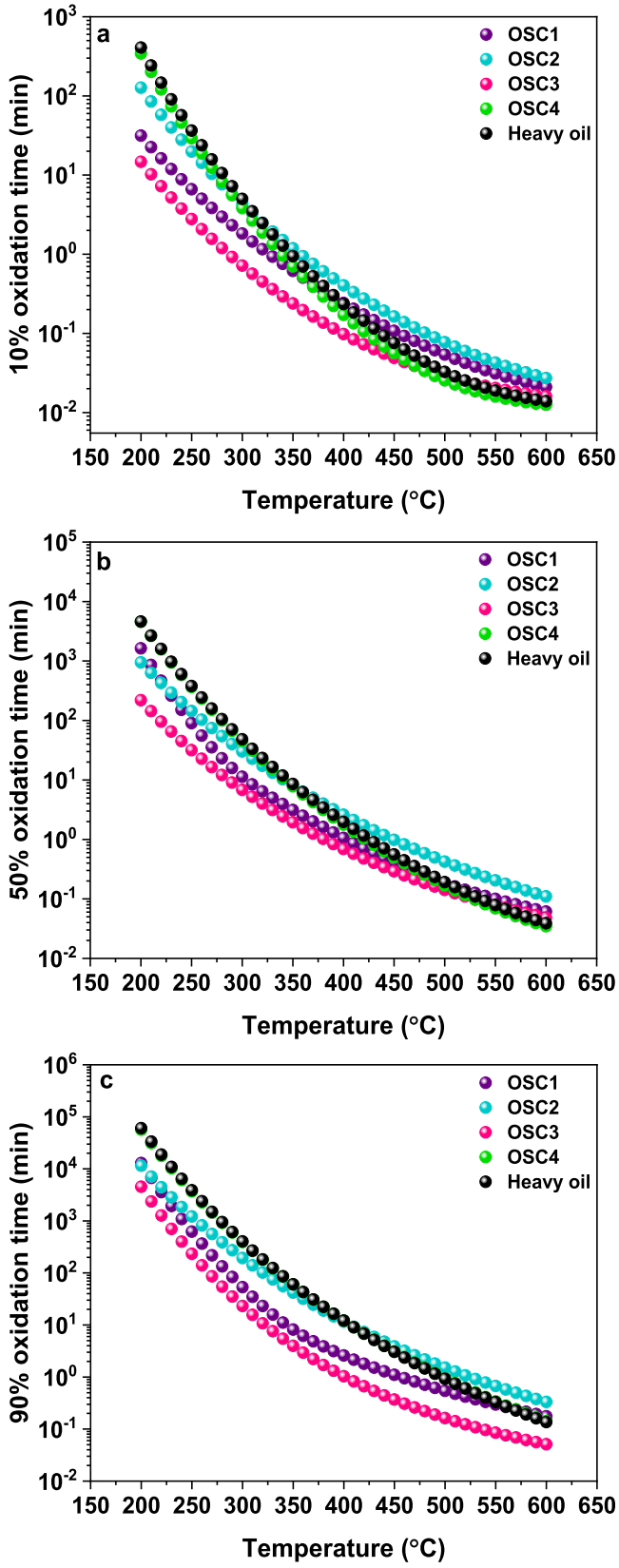

Figure 10. Calculated oxidation times of heavy oil in the presence and absence of catalysts for (a) 10%, (b) 50%, and (c) 90% oxidation conversion.

smaller clusters show higher reactivity.[69] In this study, a trimer metal cluster of Cu was considered. The optimized structure of

https://doi.org/10.1021/acs.iecr.1c03276
Ind. Eng. Chem. Res. 2021, 60, 14713−14727

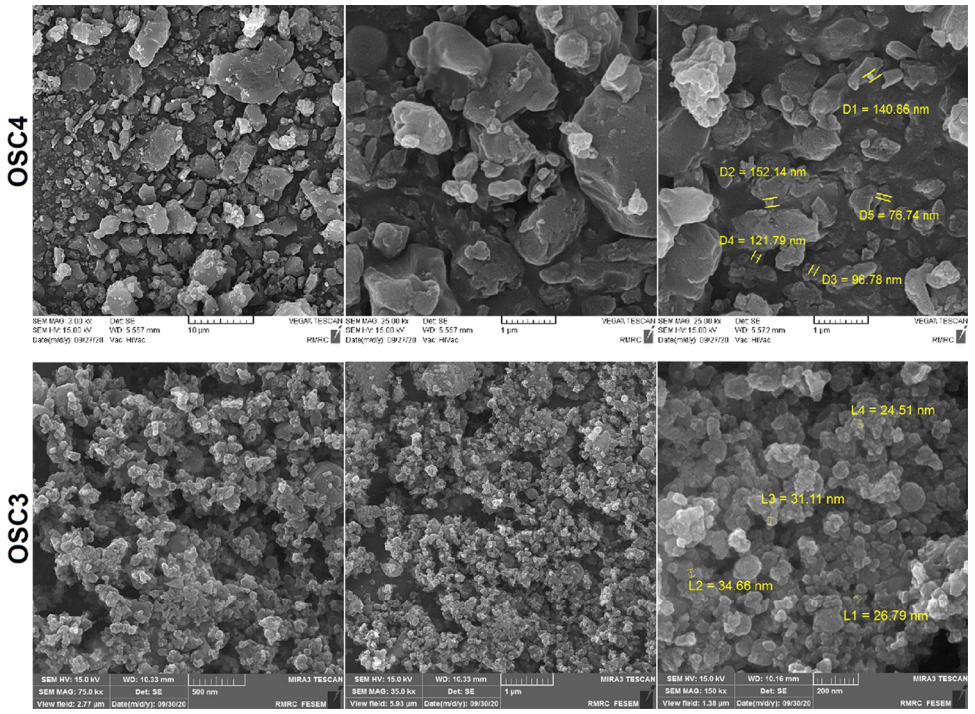

Figure 11. Morphology of Cu and Ni nanoparticles in OSC3 and OSC4.

the Cu_3 cluster has a near-D_{3h} symmetry with an angle of 70.0°, a dipole moment of 0.56 Debye, and a Cu−Cu bond length of 2.34 Å. Furthermore, the optimized structure of the Ni_3 cluster has D_{3h} symmetry, with an angle of 59.9°, a dipole moment of 0 Debye, and a Ni−Ni bond length of 2.22 Å. The results of this section are in good agreement with the results obtained from high-level computational methods [CAM-B3LYP/(14s,9p,5d,1f)].[59] A summary of the results related to the optimization of Cu and Ni cluster structures is given in Table 5. In the study of large molecular systems that contain a large number of atoms, various solutions such as using the molecular dynamics method or an alternative molecular model are used due to the reduction of computational costs.[70,71] The optimized structure of COL2 and oleic acid studied is shown in Figure 13. The structure shown in Figure 13a is considered the high-performance ligand (according to the obtained results from DSC and TGA analyses), and its performance was evaluated based on the amount of binding energy required to interact with the metal cluster with the commonly used oleic acid that is shown in Figure 13b.

The COL2 structure was simplified as a single chain equivalent to the oleic acid because it has three branches that can interact with a metal cluster and a large number of atoms. This structure is shown in Figure 13c. The quantum parameters for structure optimization are summarized in Table 5. As can be seen, the complex of COL2 with a Cu metal cluster (complex-1) has a lower energy level than the complex of oleic acid with it (complex-2), the difference of which is about −54.8 kcal/mol. The predicted binding energy for complex-1 is about −118.7 kcal/mol, considering that there is a possibility of interaction from three similar points at the same time, and about −63.9 kcal/mol for complex-2, which provides only one possibility for interaction. Such a significant difference is related to the nature of the interaction of COL2 with the Cu cluster and the number of points of interaction that is discussed later. In addition, the interaction of COL2 with a Ni cluster (complex-3) was investigated, which predicted that the binding energy of their interaction was about −95.6 kcal/mol. Therefore, it can be concluded that, first, COL2 has a stronger interaction than oleic acid with the same metal cluster of Cu, and second, the interaction of this new ligand with a Cu cluster is much more favorable than a Ni cluster.

The energy gap is usually considered a measure of the stability of a structure.[72] A greater energy gap represents a more stable structure and vice versa. The energy gap values for complex-1, complex-2, and complex-3 are 1.9, 1.17, and 1.48 eV, respectively. It is highlighted that the complex formed with COL2 has more stability for both Cu and Ni metal clusters than the complex formed with a common ligand such as oleic acid. In other words, for a similar metal cluster (Cu cluster), COL2 showed a more stable interaction than oleic acid. The energy gap is related to the energy difference between HOMOs and LUMOs, which are depicted in Figure 14. These orbitals represent the active area that is involved in reactions and interactions. This energy difference of molecular orbitals is about 3.28 for COL2 and 2.43 eV for oleic acid.

Molecular electrostatic potential (MEP) energy levels are important in understanding the relationship between potential energy and the molecular structure, as well as the positioning of structures in creating interactions with each other. Figure 15 shows the MEP energy levels of COL2, oleic acid, and Cu cluster structures. The red, yellow, and blue areas represent negative, neutral, and positive potential energy levels.[73] Using MEP, it can be predicted that the interaction of both ligands can be formed through their carboxyl group with the metal cluster.

As noted, NBO analysis is a fundamental method for examining the nature of interactions; therefore, a second-order perturbation analysis of the Fock matrix was performed to evaluate NBO-based donor−acceptor interactions between ligand and metal. These interactions result in the loss of local

https://doi.org/10.1021/acs.iecr.1c03276
Ind. Eng. Chem. Res. 2021, 60, 14713−14727

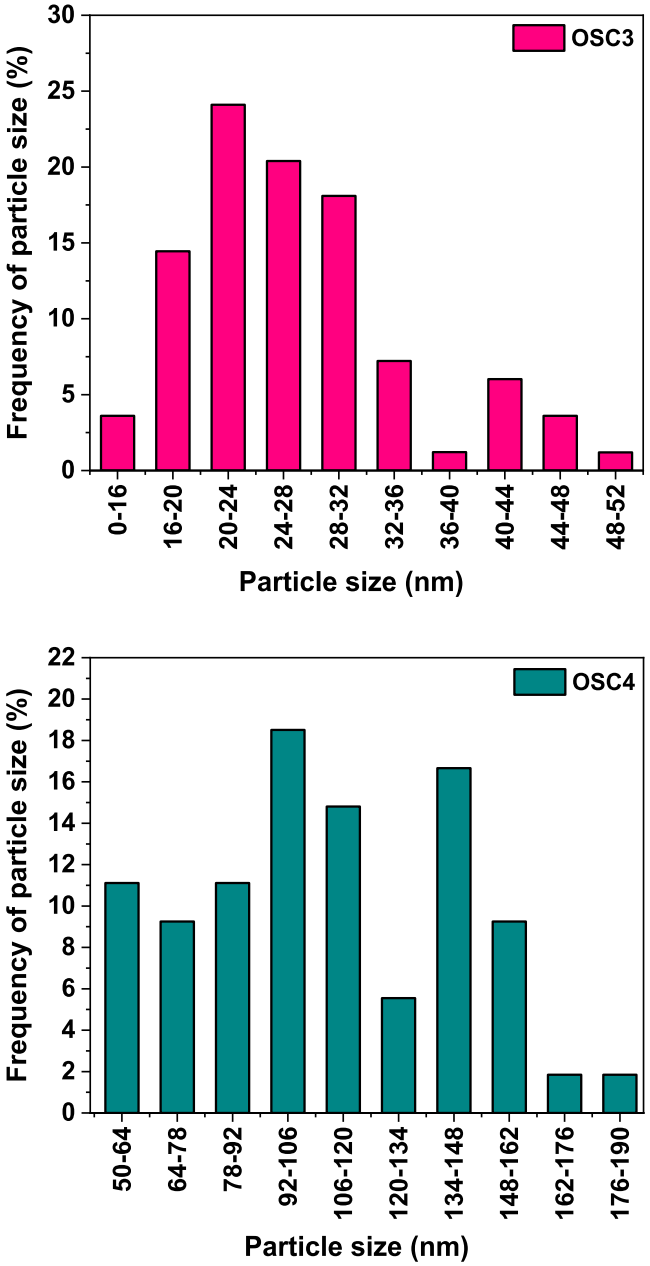

Figure 12. Frequency graphs of the particle size of Cu and Ni nanoparticles in OSC3 and OSC4.

NBOs that occupy the Lewis ideal structure for discharging non-Lewis circuits. In other words, they denote the delocalization of electrons.[74,75] For each donor NBO (i) and acceptor NBO (j), the stabilization energy $E(2)$ associated with delocalization $i \rightarrow j$ is estimated as

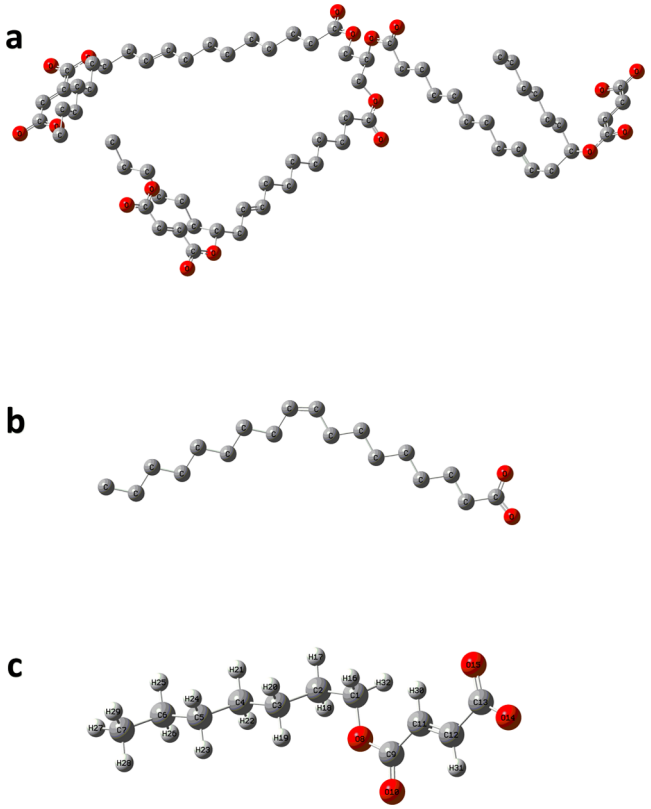

Figure 13. Optimized structures of COL2 (a), oleic acid (b), and simplified COL2(c).

$$E(2) = q_i \frac{F(i.\ j)^2}{\varepsilon_j - \varepsilon_i} \tag{7}$$

where q_i is the donor orbital occupancy (usually is 2), $\varepsilon_i$and ε_j are diagonal elements (orbital energies), and $F(i, j)$ is the off-diagonal NBO Fock matrix element.[76] If the amount of the stabilization energy, $E(2)$, is high, it can be concluded that the charge transfer between the donor and the acceptor is more and the interaction is strong. A summary of the results of the NBO analysis is listed in Table 6.

As seen in Table 6, the charge transfer of $\sigma_{O15-Cu33} \rightarrow \sigma^*_{C13-O14}$ with stabilization energy of 38.4 kcal/mol for complex-1 reveals an intense charge transfer that predicts a strong interaction between Cu−O and C−O. This charge transfer and also the charge transfer of $n_{O15} \rightarrow \sigma^*_{O15-Cu33}$ represent a chemical bond between the oxygen atom of the carboxylic acid group (O15) in the COL2 structure and the Cu atom of the cluster group (Cu33). Moreover, the charge transfer of $n_{O14} \rightarrow n^*_{Cu34}$ with stabilization energy of about 10 kcal/mol implies a strong interaction between the oxygen atom

Table 5. Summary of Structure Optimization Results and Energy Calculation

structure	energy (H)	HOMO (H)	LUMO (H)	E_{gap} (eV)	momentum (Debye)	E_b (H)	E_b (kcal/mol)
complex-1	−5652.30	−0.020	0.050	1.90	73.51	−0.19	−118.7
COL2	−730.40	−0.039	0.082	3.28	73.22		
complex-2	−5503.06	0.026	0.069	1.17	48.24	−0.10	−63.9
oleic acid	−581.12	−0.008	0.081	2.43	35.46		
complex-3	−5255.57	−0.032	0.023	1.48	12.10	−0.15	−95.6
Cu cluster	−4921.84	−0.151	−0.105	1.26	0.56		
Ni cluster	−4525.12	−0.172	−0.092	2.18	0.00		

https://doi.org/10.1021/acs.iecr.1c03276
Ind. Eng. Chem. Res. 2021, 60, 14713−14727

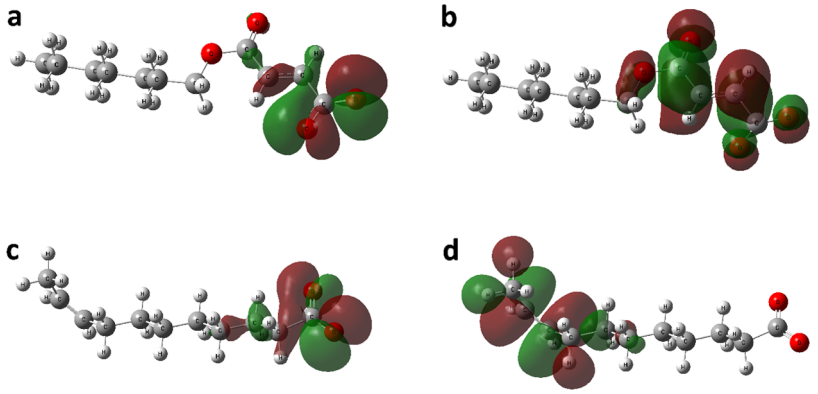

Figure 14. HOMOs (a) and LUMOs (b) of COL2 and HOMOs (c) and LUMOs (d) of oleic acid.

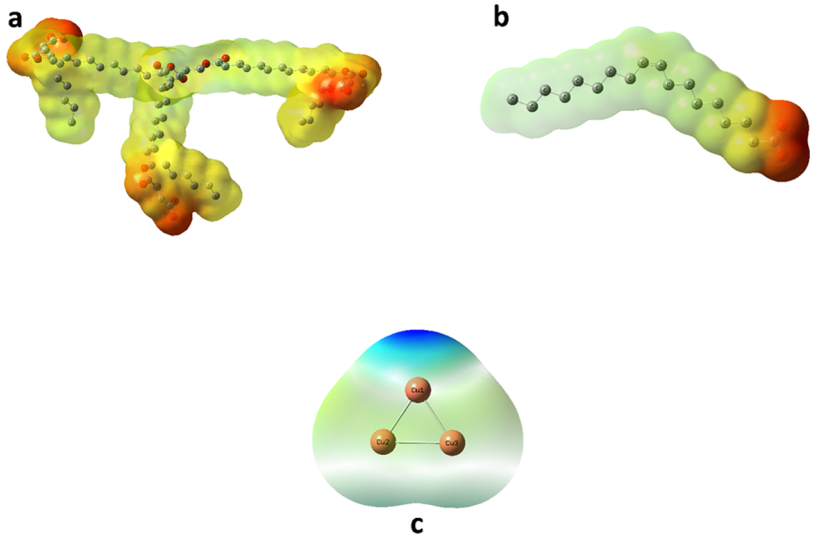

Figure 15. Molecular electrostatic potential energy levels of COL2 (a), oleic acid (b), and Cu cluster.

Table 6. Features Based on NBO Analysis to Calculate Charge Transfer

complex	bond	charge transfer	$E(2)$ (kcal/mol)
complex-1	Cu33−O15	$\sigma_{O15-Cu33} \rightarrow \sigma^*_{C13-O14}$	38.41
	C13−O15	$n_{O15} \rightarrow \sigma^*_{O15-Cu33}$	4.47
	C13−O14	$n_{O14} \rightarrow n^*_{Cu34}$	10.16
	C11═C12	$\sigma_{C11-C12} \rightarrow n^*_{Cu35}$	4.63
	Cu35−Cu33	$n_{Cu35} \rightarrow \sigma^*_{O15-Cu33}$	40.73
complex-2	C1−O12	$n_{O12} \rightarrow \sigma^*_{Cu34-Cu35}$	5.97
	C1−O13	$n_{O13} \rightarrow n^*_{Cu33}$	10.91

of the carboxylic group (O14) in COL2 and the Cu atom of the cluster group (Cu34). The charge transfer of $\sigma_{C11-C12} \rightarrow n^*_{Cu35}$ with stabilization energy of about 4.6 kcal/mol predicts that the C11 ═ C12 bond with the Cu cluster has a significant interaction. In complex-2, there are two significant charges, but its total stabilization energy is much less than that of complex-1. In topological QTAIM analysis, the nature of bonding is analyzed by properties of electron density (ρ) and its derivatives. The Laplacian of electron density ($\nabla^2\rho$) at the BCP is related to the bond interaction energy by expression of the virial theorem. Negative Laplacian ($\nabla^2\rho < 0$) demonstrates the extra potential energy in BCP. This means that the electronic charge is concentrated in the internuclear region and shared by two nuclei (this is common for covalent interactions). Positive Laplacian ($\nabla^2\rho > 0$) in BCP signifies a decrease in electronic charge along the bond path, and this is an illustration of the electrostatic interaction. In addition, Hamiltonian (H) as the electronic energy density evaluated at a BCP can be used to compare the kinetic and potential energy densities.[77] For all interactions with significant electron sharing, H is negative, and its absolute value expresses the covalent character of the interaction. In this study, a common interaction that exists in both complexes (Cu−O) was evaluated, and the results are shown in Table 7.

Table 7. QTAIM Analysis of Cu−O in Both Complexes

complex	BCP	ρ	Laplacian ($\nabla^2\rho$)	Hamiltonian (H)
complex-1	BCP1	0.06	−0.08	−0.002
complex-2	BCP2	0.02	−0.01	−0.001

A comparison of the electron density values (ρ) for complexes 1 and 2 (equals 0.06 for BCP1 and 0.02 for BCP2) is consistent with their binding energies because, as expected, a strong bond is usually associated with a high electron density in BCP. Furthermore, the negative value of Laplacian ($\nabla^2\rho$) for Cu−O bonds indicates that this interaction should be classified as a covalent type of bonding. The negative values of H for all BCPs imply the covalent nature of the corresponding bonds. By comparing the values of

https://doi.org/10.1021/acs.iecr.1c03276
Ind. Eng. Chem. Res. 2021, 60, 14713−14727

the BCP parameters in both complexes, it can be concluded that the Cu−O bond in complex-1 has a covalent nature that is stronger with higher binding energy than the Cu−O bond in complex-2. The results of quantum calculations clearly confirm that according to the bond energy of complexes 1−3, which are −118.7, −95.6, and −63.9 kcal/mol, respectively, it can be predicted that the bonding of COL2 with the Cu metal cluster is more favorable than its bonding with the Ni metal cluster. In another comparison, it was revealed that the binding of COL2 is more favorable than that of a common ligand such as oleic acid with the Cu metal cluster. The energy gap values for complexes 1−3 are 1.9, 1.17, and 1.48 eV, respectively. These values proved that the electronic structure stability of the COL2 complex with Cu and Ni metal clusters is higher than that of the oleic acid complex with the Cu cluster. NBO calculations showed that the major contribution of the interaction of both ligands with the Cu metal cluster is due to the Cu−O bond, which is stronger for COL2. Besides, in the interaction of COL2 with the Cu metal cluster, a contribution of the interaction of the double bond of carbon with the Cu metal cluster is observed, Cu−C═C. QTAIM calculations also indicated that the covalent nature between oxygen and copper is greater for COL2.

CONCLUSIONS

Although oil-soluble catalysts with different metals have been investigated for in situ oxidation of heavy oil in recent years, the combined effects of ligand and metal and their interactions on the oxidation process are poorly understood. Here, we aim to fill this gap of knowledge by examining the effect of the ligand structure on the kinetics of the heavy oil oxidation process by means of thermal analysis, computational methods, and NBO and QTAIM analyses. This work has led us to conclude that the synthesized biobased catalysts could revolutionize our understanding of the heavy oil in situ combustion process and improve green enhanced oil recovery methods for better environmental protection. The results of this study indicated that the designed ligands affected the process of heavy oil oxidation differently where COL2 showed short conversion times, which corresponded to higher values of oil oxidation reaction rate relative to COL1. Besides, the efficiency of COL2 increased in the presence of Cu, where complex OSC3 containing COL2 and Cu metal not only increased the reaction rate significantly but also decreased the energy of activation of the associated process as well. A consequence of this effect is the possibility of higher thermal stability of COL2 and its higher interaction with Cu compared to the Ni cluster as demonstrated by computational methods, and NBO and QTAIM analyses of Cu−O in both complexes. This research has underlined the importance of designing new biobased catalysts for the oil industry that may have a positive impact on the environment unlike conventional catalysts that have been used during the last century. Our investigation in this area is still ongoing and seems likely to confirm our hypothesis. We deeply believe that these findings add to a growing body of literature on our understanding of the heavy oil combustion process for improving the world energy demand through exploitation of unconventional oil reserves.

ASSOCIATED CONTENT

Supporting Information

The Supporting Information is available free of charge at https://pubs.acs.org/doi/10.1021/acs.iecr.1c03276.

Kinetic parameters of the heavy oil oxidation process in the presence and absence of catalysts obtained using the model approach of nonisothermal kinetics during experiments (PDF)

AUTHOR INFORMATION

Corresponding Authors

Mohammed A. Khelkhal − *Institute of Geology and Oil & Gas Technologies, Kazan Federal University, Kazan 420008, Russia*; orcid.org/0000-0001-7922-4004; Email: aminekhelkhal@gmail.com

Arash Tajik − *Department of Petroleum Engineering, Kazan Federal University, 420008 Kazan, Russian Federation*; Email: Atajik1989@gmail.com

Semen E. Lapuk − *Institute of Geology and Oil & Gas Technologies, Kazan Federal University, Kazan 420008, Russia*; Email: lapuksemen@gmail.com

Alexey V. Vakhin − *Institute of Geology and Oil & Gas Technologies, Kazan Federal University, Kazan 420008, Russia*; orcid.org/0000-0002-5168-7063; Email: Vahin-a_v@mail.ru

Authors

Abdolreza Farhadian − *Department of Polymer & Materials Chemistry, Faculty of Chemistry and Petroleum Science, Shahid Beheshti University, 1983969411 Tehran, Iran; Department of Petroleum Engineering, Kazan Federal University, 420008 Kazan, Russian Federation*; orcid.org/0000-0002-7566-5184

Morteza Rezaeisadat − *Department of Chemistry, University of Isfahan, 81746-73441 Isfahan, Iran*

Alexey A. Eskin − *Institute of Geology and Oil & Gas Technologies, Kazan Federal University, Kazan 420008, Russia*

Nikolay O. Rodionov − *Department of Petroleum Engineering, Kazan Federal University, 420008 Kazan, Russian Federation*

Complete contact information is available at: https://pubs.acs.org/10.1021/acs.iecr.1c03276

Notes

The authors declare no competing financial interest.

ACKNOWLEDGMENTS

This work was supported by the Ministry of Science and Higher Education of the Russian Federation under agreement No. 075-15-2020-931 within the framework of the development program for a world-class Research Center "Efficient development of the global liquid hydrocarbon reserves".

REFERENCES

(1) Nemati Zadeh Haghighi, A.; Dabiri, A.; Azdarpour, A.; Karaei, M. A. Oxidation Behavior and Kinetics of Iranian Crude Oil Samples Using Thermal Analysis (TA). *Energy Sources, Part A* **2019**, 1−13.

(2) Suwaid, M. A.; Varfolomeev, M. A.; Al-muntaser, A. A.; Yuan, C.; Starshinova, V. L.; Zinnatullin, A.; Vagizov, F. G.; Rakhmatullin, I. Z.; Emelianov, D. A.; Chemodanov, A. E. In-Situ Catalytic Upgrading of Heavy Oil Using Oil-Soluble Transition Metal-Based Catalysts. *Fuel* **2020**, *281*, No. 118753.

(3) Omajali, J. B.; Hart, A.; Walker, M.; Wood, J.; Macaskie, L. E. In-Situ Catalytic Upgrading of Heavy Oil Using Dispersed Bionanoparticles Supported on Gram-Positive and Gram-Negative Bacteria. *Appl. Catal., B* **2017**, *203*, 807−819.

(4) Jameel, A. G. A.; Khateeb, A.; Elbaz, A. M.; Emwas, A.-H.; Zhang, W.; Roberts, W. L.; Sarathy, S. M. Characterization of Deasphalted Heavy Fuel Oil Using APPI (+) FT-ICR Mass Spectrometry and NMR Spectroscopy. *Fuel* **2019**, *253*, 950−963.
(5) Sheng, J. J. *Modern Chemical Enhanced Oil Recovery: Theory and Practice*; Gulf Professional Publishing, 2010.
(6) Mahmoud, T.; Samak, N. A.; Abdelhamid, M. M.; Aboulrous, A. A.; Xing, J. Modification Wettability and Interfacial Tension of Heavy Crude Oil by Green Bio-Surfactant Based on Bacillus Licheniformis and Rhodococcus Erythropolis Strains under Reservoir Conditions: Microbial Enhanced Oil Recovery. *Energy Fuels* **2021**, *35*, 1648−1663.
(7) Shi, L.; Liu, C.; Chen, M.; Hua, Z.; Ye, Z.; Zhang, J. Synthesis and Evaluation of a Hyperbranched Copolymer as Viscosity Reducer for Offshore Heavy Oil. *J. Pet. Sci. Eng.* **2021**, *196*, No. 108011.
(8) Baek, K. H.; Argüelles-Vivas, F. J.; Abeykoon, G. A.; Okuno, R.; Weerasooriya, U. P. Low-Tension Polymer Flooding Using a Short-Hydrophobe Surfactant for Heavy Oil Recovery. *Energy Fuels* **2020**, *34*, 15936−15948.
(9) Bhicajee, P.; Romero-Zerón, L. Effect of Different Low Salinity Flooding Schemes and the Addition of Alkali on the Performance of Low-Salinity Waterflooding during the Recovery of Heavy Oil from Unconsolidated Sandstone. *Fuel* **2021**, *289*, No. 119981.
(10) Wu, X.; Zhang, Y.; Zhang, K.; Liu, B.; Zuo, J. Y.; Chen, G.; Xiao, P. An Experimental Investigation of Liquid CO2-in-Water Emulsions for Improving Oil Recovery. *Fuel* **2021**, *288*, No. 119734.
(11) Pirizadeh, M.; Alemohammad, N.; Manthouri, M.; Pirizadeh, M. A New Machine Learning Ensemble Model for Class Imbalance Problem of Screening Enhanced Oil Recovery Methods. *J. Pet. Sci. Eng.* **2021**, *198*, No. 108214.
(12) Alade, O. S.; Al Shehri, D.; Mahmoud, M.; Mokheimer, E. M. A.; Al Hamad, J.; Kamal, M. S.; Al-Nakhli, A.; Sasaki, K. A Novel Technique for Heavy Oil Recovery Using Poly Vinyl Alcohol (PVA) and PVA-NaOH with Ethanol Additive. *Fuel* **2021**, *285*, No. 119128.
(13) Mehrabi-Kalajahi, S.; Varfolomeev, M. A.; Yuan, C.; Zinnatullin, A. L.; Rodionov, N. O.; Vagizov, F. G.; Osin, Y. N.; Yakimova, L. S. Improving Heavy Oil Oxidation Performance by Oil-Dispersed CoFe2O4 Nanoparticles in In-Situ Combustion Process for Enhanced Oil Recovery. *Fuel* **2021**, *285*, No. 119216.
(14) Azarhava, H.; Jafari, A.; Vakilchap, F.; Mousavi, S. M. Stability and Performance of Poly γ-(Glutamic Acid) in the Presence of Sulfate Ion for Enhanced Heavy Oil Recovery. *J. Pet. Sci. Eng.* **2021**, *196*, No. 107688.
(15) Fan, J.; Yang, J.; Fan, X.; Wu, L. Experimental Study on the Mechanism of Enhanced Oil Recovery by Non-Condensable Gas-Assisted Steam Flooding Process in Extra-Heavy Oil Reservoir. *Energy Sources, Part A* **2021**, *43*, 444−460.
(16) Babadagli, T. Philosophy of EOR. *J. Pet. Sci. Eng.* **2020**, *188*, No. 106930.
(17) Yuan, C.; Emelianov, D. A.; Varfolomeev, M. A. Oxidation Behavior and Kinetics of Light, Medium, and Heavy Crude Oils Characterized by Thermogravimetry Coupled with Fourier Transform Infrared Spectroscopy. *Energy Fuels* **2018**, *32*, 5571−5580.
(18) Yuan, C.; Emelianov, D. A.; Varfolomeev, M. A.; Rodionov, N. O.; Suwaid, M. A.; Vakhitov, I. R. Mechanistic and Kinetic Insight into Catalytic Oxidation Process of Heavy Oil in In-Situ Combustion Process Using Copper (II) Stearate as Oil Soluble Catalyst. *Fuel* **2021**, *284*, No. 118981.
(19) Chu, Y.; Fan, C.; Zhang, Q.; Zan, C.; Ma, D.; Jiang, H.; Wang, Y.; Wei, F. The Oxidation of Heavy Oil to Enhance Oil Recovery: The Numerical Model and the Criteria to Describe the Low and High Temperature Oxidation. *Chem. Eng. J.* **2014**, *248*, 422−429.
(20) Zhao, S.; Pu, W.; Peng, X.; Zhang, J.; Ren, H. Low-Temperature Oxidation of Heavy Crude Oil Characterized by TG, DSC, GC-MS, and Negative Ion ESI FT-ICR MS. *Energy* **2021**, *214*, No. 119004.
(21) Jameel, A. G. A.; Han, Y.; Brignoli, O.; Telalović, S.; Elbaz, A. M.; Im, H. G.; Roberts, W. L.; Sarathy, S. M. Heavy Fuel Oil Pyrolysis and Combustion: Kinetics and Evolved Gases Investigated by TGA-FTIR. *J. Anal. Appl. Pyrolysis* **2017**, *127*, 183−195.
(22) Elbaz, A. M.; Gani, A.; Hourani, N.; Emwas, A.-H.; Sarathy, S. M.; Roberts, W. L. TG/DTG, FT-ICR Mass Spectrometry, and NMR Spectroscopy Study of Heavy Fuel Oil. *Energy Fuels* **2015**, *29*, 7825−7835.
(23) Elbaz, A. M.; Khateeb, A. A.; Roberts, W. L. PM from the Combustion of Heavy Fuel Oils. *Energy* **2018**, *152*, 455−465.
(24) Li, Y.; Wang, Z.; Hu, Z.; Xu, B.; Li, Y.; Pu, W.; Zhao, J. A Review of in Situ Upgrading Technology for Heavy Crude Oil. *Petroleum* **2021**, *7*, 117−122.
(25) Yuan, C.; Mehrabi-Kalajahi, S. S.; Sadikov, K.; Varfolomeev, M. A.; Emelianov, D. A.; Rodionov, N. O.; Amerkhanov, M. I. In *Potential of Copper-Based Oil Soluble Catalyst for Improving Efficiency of In-Situ Combustion Process: Catalytic Combustion, Catalytic In-Situ Oil Upgrading, and Increased Oil Recovery*, SPE Kuwait Oil & Gas Show and Conference, Society of Petroleum Engineers, 2019.
(26) Yuan, C.; Sadikov, K.; Varfolomeev, M.; Khaliullin, R.; Pu, W.; Al-Muntaser, A.; Mehrabi-Kalajahi, S. S. Low-Temperature Combustion Behavior of Crude Oils in Porous Media under Air Flow Condition for in-Situ Combustion (ISC) Process. *Fuel* **2020**, *259*, No. 116293.
(27) Yuan, C.; Emelianov, D. A.; Varfolomeev, M. A.; Abaas, M. Comparison of Oxidation Behavior of Linear and Branched Alkanes. *Fuel Process. Technol.* **2019**, *188*, 203−211.
(28) Maity, S. K.; Ancheyta, J.; Marroquín, G. Catalytic Aquathermolysis Used for Viscosity Reduction of Heavy Crude Oils: A Review. *Energy Fuels* **2010**, *24*, 2809−2816.
(29) Yuan, C.; Varfolomeev, M. A.; Emelianov, D. A.; Suwaid, M. A.; Khachatrian, A. A.; Starshinova, V. L.; Vakhitov, I. R.; Al-Muntaser, A. A. Copper Stearate as a Catalyst for Improving the Oxidation Performance of Heavy Oil in In-Situ Combustion Process. *Appl. Catal., A* **2018**, *564*, 79−89.
(30) Khelkhal, M. A.; Eskin, A. A.; Sitnov, S. A.; Vakhin, A. V. Impact of Iron Tallate on the Kinetic Behavior of the Oxidation Process of Heavy Oils. *Energy Fuels* **2019**, *33*, 7678−7683.
(31) Khelkhal, M. A.; Eskin, A. A.; Mukhamatdinov, I. I.; Feoktistov, D. A.; Vakhin, A. V. Comparative Kinetic Study on Heavy Oil Oxidation in the Presence of Nickel Tallate and Cobalt Tallate. *Energy Fuels* **2019**, *33*, 9107−9113.
(32) Khelkhal, M. A.; Eskin, A. A.; Vakhin, A. V. Kinetic Study on Heavy Oil Oxidation by Copper Tallates. *Energy Fuels* **2019**, *33*, 12690−12695.
(33) Khelkhal, M. A.; Eskin, A. A.; Nurgaliev, D. K.; Vakhin, A. V. Thermal Study on Stabilizing the Combustion Front via Bimetallic Mn@Cu Tallates during Heavy Oil Oxidation. *Energy Fuels* **2020**, *34*, 5121−5127.
(34) Li, C.; Huang, W.; Zhou, C.; Chen, Y. Advances on the Transition-Metal Based Catalysts for Aquathermolysis Upgrading of Heavy Crude Oil. *Fuel* **2019**, *257*, No. 115779.
(35) Alkhaldi, S.; Husein, M. M. Hydrocracking of Heavy Oil by Means of in Situ Prepared Ultradispersed Nickel Nanocatalyst. *Energy Fuels* **2014**, *28*, 643−649.
(36) Hosseinpour, N.; Mortazavi, Y.; Bahramian, A.; Khodatars, L.; Khodadadi, A. A. Enhanced Pyrolysis and Oxidation of Asphaltenes Adsorbed onto Transition Metal Oxides Nanoparticles towards Advanced In-Situ Combustion EOR Processes by Nanotechnology. *Appl. Catal., A* **2014**, *477*, 159−171.
(37) Amanam, U. U.; Kovscek, A. R. Analysis of the Effects of Copper Nanoparticles on In-Situ Combustion of Extra Heavy-Crude Oil. *J. Pet. Sci. Eng.* **2017**, *152*, 406−415.
(38) Al-Attas, T. A.; Ali, S. A.; Zahir, M. H.; Xiong, Q.; Al-Bogami, S. A.; Malaibari, Z. O.; Razzak, S. A.; Hossain, M. M. Recent Advances in Heavy Oil Upgrading Using Dispersed Catalysts. *Energy Fuels* **2019**, *33*, 7917−7949.
(39) Yusuf, A.; Al-Hajri, R. S.; Al-Waheibi, Y. M.; Jibril, B. Y. In-Situ Upgrading of Omani Heavy Oil with Catalyst and Hydrogen Donor. *J. Anal. Appl. Pyrolysis* **2016**, *121*, 102−112.
(40) Petrukhina, N. N.; Kayukova, G. P.; Romanov, G. V.; Tumanyan, B. P.; Foss, L. E.; Kosachev, I. P.; Musin, R. Z.; Ramazanova, A. I.; Vakhin, A. V. Conversion Processes for High-

https://doi.org/10.1021/acs.iecr.1c03276
Ind. Eng. Chem. Res. 2021, 60, 14713−14727

Viscosity Heavy Crude Oil in Catalytic and Noncatalytic Aquathermolysis. *Chem. Technol. Fuels Oils* **2014**, *50*, 315−326.
(41) Zhao, J.; Liu, Y. J.; Chen, Q. Y. Upgrading Heavy Oil by Catalytic Aquathermolysis Using Formic Acid as Hydrogen Donor. In *Advanced Materials Research*; Trans Tech Publications, 2011; Vol. *236*, pp 844−849.
(42) Zhao, F.; Liu, Y.; Fu, Z.; Zhao, X. Using Hydrogen Donor with Oil-Soluble Catalysts for Upgrading Heavy Oil. *Russ. J. Appl. Chem.* **2014**, *87*, 1498−1506.
(43) Qin, W. L.; Xiao, Z. L. The Researches on Upgrading of Heavy Crude Oil by Catalytic Aquathermolysis Treatment Using a New Oil-Soluble Catalyst. In *Advanced Materials Research*; Trans Tech Publications, 2013; Vol. *608*, pp 1428−1432.
(44) Bagheri, S. R.; Gray, M. R.; Shaw, J. M.; McCaffrey, W. C. In Situ Observation of Mesophase Formation and Coalescence in Catalytic Hydroconversion of Vacuum Residue Using a Stirred Hot-Stage Reactor. *Energy Fuels* **2012**, *26*, 3167−3178.
(45) Khelkhal, M.; Eskin, A.; Vakhin, A. In *A Comparative Study of Heavy Oil Oxidation Thermal Behavior in the Presence of Cu-Mn Tallates*, IOP Conference Series: Earth and Environmental Science, IOP Publishing, 2019; p 12013.
(46) Farhadian, A.; Ahmadi, A.; Omrani, I.; Miyardan, A. B.; Varfolomeev, M. A.; Nabid, M. R. Synthesis of Fully Bio-Based and Solvent Free Non-Isocyanate Poly (Ester Amide/Urethane) Networks with Improved Thermal Stability on the Basis of Vegetable Oils. *Polym. Degrad. Stab.* **2018**, *155*, 111−121.
(47) Natarajan, J.; Rattan, S.; Singh, U.; Madras, G.; Chatterjee, K. Polyanhydrides of Castor Oil−Sebacic Acid for Controlled Release Applications. *Ind. Eng. Chem. Res.* **2014**, *53*, 7891−7901.
(48) Vyazovkin, S.; Burnham, A. K.; Criado, J. M.; Pérez-Maqueda, L. A.; Popescu, C.; Sbirrazzuoli, N. ICTAC Kinetics Committee Recommendations for Performing Kinetic Computations on Thermal Analysis Data. *Thermochim. Acta* **2011**, *520*, 1−19.
(49) Lapuk, S. E.; Zubaidullina, L. S.; Ziganshin, M. A.; Mukhametzyanov, T. A.; Schick, C.; Gerasimov, A. V. Kinetic Stability of Amorphous Solid Dispersions with High Content of the Drug: A Fast Scanning Calorimetry Investigation. *Int. J. Pharm.* **2019**, *562*, 113−123.
(50) Kissinger, H. E. Reaction Kinetics in Differential Thermal Analysis. *Anal. Chem.* **1957**, *29*, 1702−1706.
(51) Friedman, H. L. Kinetics of Thermal Degradation of Char-forming Plastics from Thermogravimetry. Application to a Phenolic Plastic. In *Journal of Polymer Science Part C: Polymer Symposia*; Wiley Online Library, 1964; Vol. *6*, pp 183−195.
(52) Lapuk, S. E.; Mukhametzyanov, T. A.; Schick, C.; Gerasimov, A. V. Crystallization Kinetics and Glass-Forming Ability of Rapidly Crystallizing Drugs Studied by Fast Scanning Calorimetry. *Int. J. Pharm.* **2021**, *599*, No. 120427.
(53) Lapuk, S. E.; Mukhametzyanov, T. A.; Schick, C.; Gerasimov, A. V. Kinetic Stability of Amorphous Dipyridamole: A Fast Scanning Calorimetry Investigation. *Int. J. Pharm.* **2020**, *574*, No. 118890.
(54) Farhadian, A.; Varfolomeev, M. A.; Rezaeisadat, M.; Semenov, A. P.; Stoporev, A. S. Toward a Bio-Based Hybrid Inhibition of Gas Hydrate and Corrosion for Flow Assurance. *Energy* **2020**, *210*, No. 118549.
(55) Kohn, W.; Sham, L. J. Self-Consistent Equations Including Exchange and Correlation Effects. *Phys. Rev.* **1965**, *140*, A1133−A1138.
(56) Lee, C.; Yang, W.; Parr, R. G. Density-Functional Exchange-Energy Approximation with Correct Asymptotic Behaviour. *Phys. Rev. B* **1988**, *37*, 785−789.
(57) Dunning, T. H., Jr. Gaussian Basis Sets for Use in Correlated Molecular Calculations. I. The Atoms Boron through Neon and Hydrogen. *J. Chem. Phys.* **1989**, *90*, 1007−1023.
(58) Miertuš, S.; Scrocco, E.; Tomasi, J. Electrostatic Interaction of a Solute with a Continuum. A Direct Utilizaion of AB Initio Molecular Potentials for the Prevision of Solvent Effects. *Chem. Phys.* **1981**, *55*, 117−129.
(59) Jamshidi, Z.; Farhangian, H.; Tehrani, Z. A. Glucose Interaction with Au, Ag, and Cu Clusters: Theoretical Investigation. *Int. J. Quantum Chem.* **2013**, *113*, 1062−1070.
(60) Van Duijneveldt, F. B.; van Duijneveldt-van de Rijdt, J. G. C. M.; van Lenthe, J. H. State of the Art in Counterpoise Theory. *Chem. Rev.* **1994**, *94*, 1873−1885.
(61) Reed, A. E.; Weinstock, R. B.; Weinhold, F. Natural Population Analysis. *J. Chem. Phys.* **1985**, *83*, 735−746.
(62) Reed, A. E.; Curtiss, L. A.; Weinhold, F. Intermolecular Interactions from a Natural Bond Orbital, Donor-Acceptor Viewpoint. *Chem. Rev.* **1988**, *88*, 899−926.
(63) Bader, R. F. W. *A Quantum Theory*, Clarendon: Oxford 1990.
(64) Bader, R. F. W. *AIM2000 Program Package*, version 2.0; McMaster University: Hamilton, Ontario, Canada, 2002, There is no Corresp. Rec. this Ref. Sch.
(65) Burger, J. G.; Sahuquet, B. C. Chemical Aspects of In-Situ Combustion - Heat of Combustion and Kinetics. *Soc. Pet. Eng. J.* **1972**, *12*, 410−422.
(66) Freund, J. E.; Perles, B. M. *Modern Elementary Statistics*; Pearson College Division, 2007.
(67) Heidarshenas, A.; Azizi, Z.; Peyghambarzadeh, S. M.; Sayyahi, S. Experimental Investigation of the Particle Size Effect on Heat Transfer Coefficient of Al 2 O 3 Nanofluid in a Cylindrical Microchannel Heat Sink. *J. Therm. Anal. Calorim.* **2019**, *141*, 957−967.
(68) Peng, H.; Ding, G.; Hu, H.; Jiang, W. Effect of Nanoparticle Size on Nucleate Pool Boiling Heat Transfer of Refrigerant/Oil Mixture with Nanoparticles. *Int. J. Heat Mass Transfer* **2011**, *54*, 1839−1850.
(69) Pyykkö, P. Magic Nanoclusters of Gold. *Nat. Nanotechnol.* **2007**, *2*, 273−274.
(70) Schlick, T. Molecular Modeling and Simulation: An Interdisciplinary Guide. In *Interdisciplinary Applied Mathematics*; Springer Science & Business Media, 2010; Vol. *21*, pp 1−723.
(71) Jensen, J. H. *Molecular Modeling Basics*; CRC Press, 2010.
(72) Joswig, J.-O.; Roy, S.; Sarkar, P.; Springborg, M. Stability and Bandgap of Semiconductor Clusters. *Chem. Phys. Lett.* **2002**, *365*, 75−81.
(73) Murray, J. S.; Politzer, P. The Electrostatic Potential: An Overview. *Wiley Interdiscip. Rev.: Comput. Mol. Sci.* **2011**, *1*, 153−163.
(74) Stone, A. J. Natural Bond Orbitals and the Nature of the Hydrogen Bond. *J. Phys. Chem. A* **2017**, *121*, 1531−1534.
(75) Weinhold, F.; Landis, C. R. Natural Bond Orbitals and Extensions of Localized Bonding Concepts. *Chem. Educ. Res. Pract.* **2001**, *2*, 91−104.
(76) Glendening, E. D.; Reed, A. E.; Carpenter, J. E.; Weinhold, F. *NBO*, version 3.1. There is no Corresp. Rec. this Ref. Sch, 1998.
(77) Bader, R. F. W. A Bond Path: A Universal Indicator of Bonded Interactions. *J. Phys. Chem. A* **1998**, *102*, 7314−7323.

https://doi.org/10.1021/acs.iecr.1c03276
Ind. Eng. Chem. Res. 2021, 60, 14713−14727